Textured Sb_2Te_3 films and GeTe/Sb_2Te_3 superlattices grown on amorphous substrates by molecular beam epitaxy

Jos E. Boschker, E. Tisbi, E. Placidi, Jamo Momand, Andrea Redaelli, Bart J. Kooi, Fabrizio Arciprete, and Raffaella Calarco

Citation: AIP Advances **7**, 015106 (2017); doi: 10.1063/1.4974464
View online: http://dx.doi.org/10.1063/1.4974464
View Table of Contents: http://aip.scitation.org/toc/adv/7/1
Published by the American Institute of Physics

Textured Sb_2Te_3 films and GeTe/Sb_2Te_3 superlattices grown on amorphous substrates by molecular beam epitaxy

Jos E. Boschker,[1] E. Tisbi,[2] E. Placidi,[2,3] Jamo Momand,[4] Andrea Redaelli,[5] Bart J. Kooi,[4] Fabrizio Arciprete,[2] and Raffaella Calarco[1,a]
[1]*Paul-Drude-Institut für Festkörperelektronik, Hausvogteiplatz 5-7, 10117 Berlin, Germany*
[2]*Dipartimento di Fisica, Università di Roma "Tor Vergata", Via della Ricerca Scientifica 1, I-00133 Rome, Italy*
[3]*CNR-ISM, Via Fosso del Cavaliere 100, I-00133 Roma, Italy*
[4]*Zernike Institute for Advanced Materials, University of Groningen, Nijenborgh 4, 9747 AG Groningen, The Netherlands*
[5]*Micron Semiconductor Italia s.r.l., Via Torri Bianche, 24, 20871 Vimercate, (MB), Italy*

(Received 11 November 2016; accepted 5 January 2017; published online 19 January 2017)

The realization of textured films of 2-dimensionally (2D) bonded materials on amorphous substrates is important for the integration of this material class with silicon based technology. Here, we demonstrate the successful growth by molecular beam epitaxy of textured Sb_2Te_3 films and GeTe/Sb_2Te_3 superlattices on two types of amorphous substrates: carbon and SiO_2. X-ray diffraction measurements reveal that the out-of-plane alignment of grains in the layers has a mosaic spread with a full width half maximum of 2.8°. We show that a good texture on SiO_2 is only obtained for an appropriate surface preparation, which can be performed by ex situ exposure to Ar^+ ions or by in situ exposure to an electron beam. X-ray photoelectron spectroscopy reveals that this surface preparation procedure results in reduced oxygen content. Finally, it is observed that film delamination can occur when a capping layer is deposited on top of a superlattice with a good texture. This is attributed to the stress in the capping layer and can be prevented by using optimized deposition conditions of the capping layer. The obtained results are also relevant to the growth of other 2D materials on amorphous substrates. [http://dx.doi.org/10.1063/1.4974464]

INTRODUCTION

2-dimensionally (2D) bonded materials, such as graphene,[1] transition metal dichalcogenides and topological insulators such as $(Bi_xSb_{1-x})_2(Se_xTe_{1-x})_3$, have a wide range of functional properties that make them attractive for future electronic devices.[2] These properties include, but are not limited to, topologically protected surface states,[3] massless Dirac fermions[4] and high figure of merit to produce thermoelectric power. Furthermore, it is recognized that this material class offers great prospects when heterostructures of these materials, so called van der Waals (vdW) heterostructures, are created.[5] A practical example of such vdW heterostructures are GeTe/Sb_2Te_3 superlattices (SL)[6–8] that are of particular interest due to their improved switching characteristics as phase change memory elements.[9] Furthermore, record high thermoelectric figures of merits have been realized in Sb_2Te_3/Bi_2Te_3 superlattices.[10]

The attractive properties of 2D materials have also resulted in a renewed interest in the epitaxy of this material class in recent years, so called vdW epitaxy.[11] This has led to an improved understanding

[a]Corresponding author: calarco@pdi-berlin.de

of vdW epitaxy. For example, it has been shown that the small interaction between film and substrate makes it possible to interface 2D materials with reconstructed semiconductor surfaces, such as the Si(1 1 1)-7×7 surface.[12,13] It has also been demonstrated that this interaction is large enough to result in coincident-lattice matching between 2D materials.[14] Furthermore, single crystalline substrates can be used for synthesizing single crystalline Bi_2Se_3 and Bi_2Te_3 layers.[15,16]

However, for the integration of 2D materials with CMOS technology it is often desirable to have a textured 2D material on top of amorphous surfaces instead of single crystalline substrate surfaces. Such surfaces can be an insulating or conductive film or a device structure with insulating and conductive area's. This is for example the case for GeTe/Sb_2Te_3 superlattices employed in phase change memory, where amorphous layers of SiO_2 and TiN are used to define the device geometry.[9] The 2D nature of materials, such as Sb_2Te_3 or Bi_2Se_3, makes it possible to obtain textured materials and a number of studies have indeed demonstrated the ability to grow textured 2D materials on amorphous substrates.[9,17–19] Saito et al. showed that the film texture can be greatly improved by using Ar^+ sputtering before the deposition in order to "clean" the substrate surface.[20] Moreover, they argued that a good texture is only obtained when there is a low reactivity between substrate and film. Nevertheless, it should be pointed out that the growth of 2D materials on amorphous substrates is still in its infancy. More detailed studies are clearly needed in order to verify these ideas and in order to improve the texture of 2D materials on amorphous substrates. Furthermore, it is not clear if the techniques developed for sputter deposition are also applicable to other deposition techniques such as molecular beam epitaxy (MBE). Finally, patterned device structures contain many different materials at the same time (e.g. W, TiN, SiN, SiO_2 and carbon). All these surfaces are exposed during deposition and may exhibit different growth properties, resulting in different properties of the grown layers.

In the present study we focused on the study on SiO_2 and carbon as representative substrate materials. We report on the realization of textured Sb_2Te_3 and GeTe/Sb_2Te_3 superlattices on amorphous carbon and SiO_2 substrates by MBE. We confirm that the texture of the layers is affected by the surface preparation by *ex situ* Ar^+ ion sputtering and show in addition that exposure to an *in situ* electron beam has a similar effect. XPS measurements on amorphous SiO_2 are performed in order to elucidate the physical origin of the improved texture on surfaces exposed to Ar^+-ions. Finally, the effect of the growth of additional layers on top of the superlattice will be investigated.

EXPERIMENTAL

Carbon films with a thickness of 30 nm grown on top of Si (0 0 1) by means of sputtering at room temperature and devices structure with a SiO_2 surface (details of the devices structures are described elsewhere[21]) were used as substrates in this study. Prior to the growth the substrates were cleaned using acetone, iso-propanol and deionized water. Ex situ argon sputter cleaning was performed using a Veeco Mark 2 HCES Ion source using an anode voltage/current of 60V/1.1-1.5A. The HCES/Ar gas flow was 3.5/6 sccm resulting a pressure of $4.9 \cdot 10^{-4}$ mbar. The emission current was 1.5 A and the neutralizing current was 0.3 A. The operating distance was chosen to be 137.5 mm. Sputtering times of 2-6 minutes were used for the devices structures. The sputtered substrates were exposed to air for a couple of hours before being introduced in the MBE system. The carbon substrates were not sputtered.

After loading the substrate in the MBE system and after degassing them, the Sb_2Te_3 films and GeTe/Sb_2Te_3 SL were grown using MBE. Single element effusion cells were used for the deposition. Additional details about the growth of Sb_2Te_3 and GeTe/Sb_2Te_3 SL can be found elsewhere.[6,7,12] Tungsten capping layers with a thickness of 50 nm were deposited *in situ* at room temperature using RF magnetron sputtering in an argon atmosphere of $3\text{-}4 \cdot 10^{-3}$ mbar. A DC bias of 97(160) V and RF power of 50(100) Watt were applied, resulting in a growth rate of 3.2(8.8) nm/min, respectively.

Structural characterization of the layers was performed by *in situ* reflection high energy electron diffraction (RHEED) using a 20 keV electron beam and by x-ray diffraction (XRD). The diffractometer is a PANalytical X'Pert Pro and uses Cu Kα_1 radiation (λ=1.540598 Å). A Hitachi S4800 scanning electron microscope was used to study the surface morphology. Transmission electron microscopy was performed using a JEOL 2010F. X-ray photoelectron spectroscopy (XPS) was performed using

an Omicron DAR 400 Al/Mg Kα nonmonochromatized X-ray source, and a VG-CLAM2 electron spectrometer. XPS measurements were performed on native SiO_2 formed on top of Si (0 0 1) wafers and on 100 nm SiO_2 deposited on top of Si(1 1 1) wafers, giving consistent results. In order to compensate for the charging of the surface the energy of the C1s peak was set to 284.8 eV.

RESULTS AND DISCUSSION

Textured Sb_2Te_3 and $GeTe/Sb_2Te_3$ superlattices on amorphous carbon

A typical RHEED pattern of an amorphous carbon substrate is shown in Fig. 1(a). The absence of diffraction peaks indicates that the substrate surface is amorphous. In order to realize $(0\ 0\ 1)_t$ (the subscript t is used to indicate that the trigonal lattice indexing is used instead of the (pseudo) cubic lattice symmetry) oriented $GeTe/Sb_2Te_3$ superlattices on amorphous substrates and patterned device substrates, an approach was used that is similar to that of Bansal et al. used for Bi_2Se_3.[17] The first Sb_2Te_3 layer of approximately 5 nm is deposited at 50°C, which is below the crystallization temperature of Sb_2Te_3 and hence the layer is amorphous. Subsequently, the temperature is raised to the deposition temperature of 227°C at a rate of 0.3 °/s. During the heating the substrate is exposed to a Te flux in order to prevent desorption of Sb_2Te_3. This results in the crystallization of the Sb_2Te_3 layer around 70°C, as can be deduced from the RHEED image taken at this temperature, i.e. Fig. 1(b). Moreover, it can be deduced from the RHEED pattern that the crystallites already have a preferred $(0\ 0\ 1)_t$ out-of-plane orientation. This preferred orientation is enhanced during the subsequent heating, as evidenced by the RHEED pattern taken at 225°C and shown in Fig. 1(c). After the preparation of this seed layer the $GeTe/Sb_2Te_3$ superlattice can be grown using standard deposition parameters for GeTe[22] and Sb_2Te_3[12] and described in detail in ref. 6. The RHEED pattern taken after the deposition of the superlattice is shown in Fig. 1(d) and confirms that the preferred orientation is maintained during the deposition. However, the coexistence of streaks corresponding to the $(1\ 0\ 0)_t$ and $(1\ 2\ 0)_t$ lattice separations in a RHEED image taken along one azimuthal angle, as indicated in Fig. 1(d), and the absence of change in the RHEED pattern upon rotation, indicates that the in-plane orientation is random.

XRD measurements were performed in order to investigate the crystal structure of the Sb_2Te_3 layers and the superlattices grown on amorphous carbon substrates. Figure 2(a) shows a linear Q_z scan of an Sb_2Te_3 layer (lower curve) and a $GeTe/Sb_2Te_3$ superlattice (upper curve). The sharp peaks due to the Si(0 0 1) substrate are easily recognized in both spectra. For the Sb_2Te_3 film, only peaks from the $(0\ 0\ 3n)_t$ family are observed, indicating that the film has a $(0\ 0\ 1)_t$ texture. The spectra of the superlattice exhibits more features, but is in good agreement with the spectra of epitaxial SL's.[6]

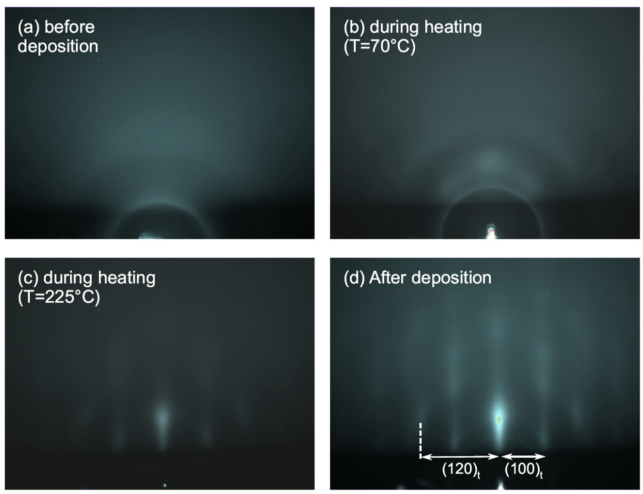

FIG. 1. RHEED patterns taken (a) before the deposition, (b)&(c) during heating and (d) after the deposition. The diffuse halo in (a) is typical for an amorphous surface and the streaky pattern in (d) is typical for a textured film with a 2D surface.

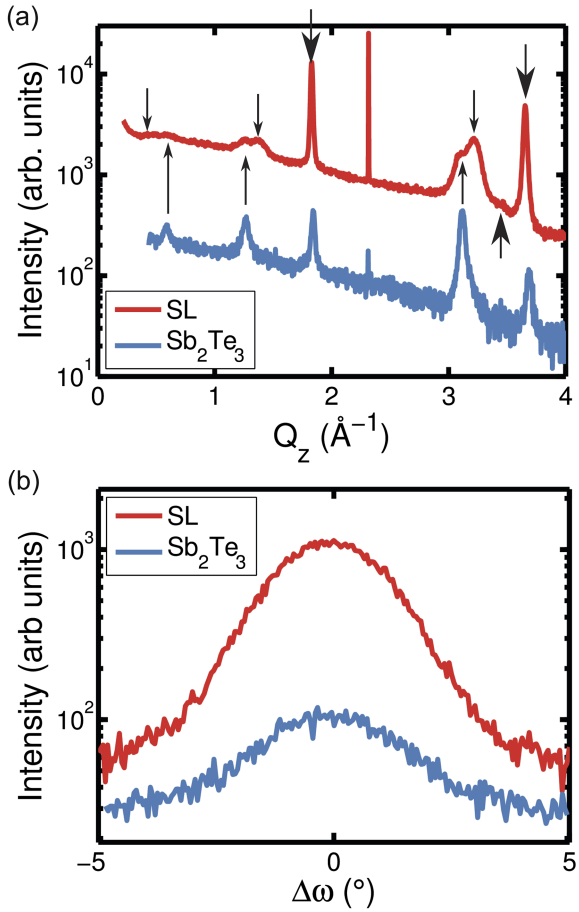

FIG. 2. Structural characterization of a Sb_2Te_3 film and a GeTe/Sb_2Te_3 SL grown on an amorphous carbon substrate. (a) linear Q_z x-ray diffraction profile of the Sb_2Te_3 film and the SL. The large arrows indicate the superlattice diffraction peaks, whereas the small downward (upward) arrows indicate the peaks due to the presence of GST (Sb_2Te_3).The large upward pointing arrow points to the SL^{-1} peak. The sharp peak around 2.3 $Å^{-1}$ is due to the Si(002) diffraction peak. (b) ω-scan around the $(0\ 0\ 9)_t$ Sb_2Te_3 peak and the first SL diffraction peak (large arrow on the left in (a)) showing a full width at half maximum of 2.8°.

This indicates that the SL also has a good texture. Furthermore, the first and second order superlattice peaks can be identified and are marked by the large downward pointing arrows. A low intensity peak can be seen on the left side of the second order superlattice peak, as indicated by the large upward pointing arrow. This peak is due to the superlattice periodicity. From the separation between this peak and the second order superlattice peak a superlattice period of 3.4 nm is determined. The fact that only one peak due to the superlattice periodicity is observed and that the intensity of this peak is weak indicate that there is a large amount of disorder in the SL. The main cause of the disorder is the mosaic spread in the out-of-plane orientation, as discussed below. Besides these peaks, three pairs of peaks are visible, which can be attributed to the presence of Sb_2Te_3 and GeTe-Sb_2Te_3 (GST) phases in the superlattice, indicated by the small upward and downward pointing arrows, respectively.[7] In order to determine the quality of the out-of-plane alignment ω-scans were performed on the $(0\ 0\ 9)_t$ peak of Sb_2Te_3 and the first order superlattice peak, i.e. Fig. 2(b). Both layers have a ω-scan with a full width half maximum (FWHM) of 2.8°. This is significantly larger than Sb_2Te_3 films or SL grown on crystalline surfaces of Si (1 1 1) substrates, which typically have a FWHM of 0.08°. Nevertheless it demonstrates that the Sb_2Te_3 film and the superlattice have a good out-of-plane alignment.

In addition, the samples were investigated by TEM in order to determine the microstructure of these layers. Figure 3(a), shows a high resolution image of the Sb_2Te_3 film. Lines running parallel to the interface with the substrate in the lower left corner are easily observed. An intensity profile taken

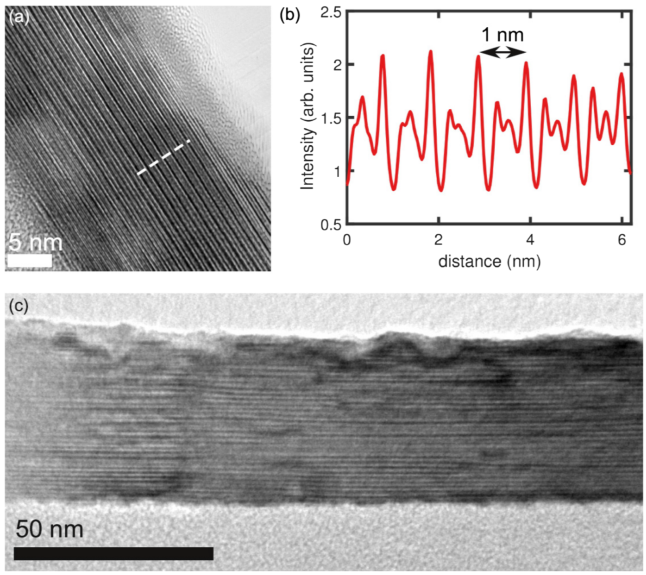

FIG. 3. TEM characterization of the Sb_2Te_3 thin film and the GeTe/Sb_2Te_3 SL grown on an amorphous carbon substrate. (a) High resolution image of the Sb_2Te_3 thin film. The dark lines that run parallel to the substrate interface are due to the vdW gaps in Sb_2Te_3 and confirm to $(0\ 0\ 1)_t$ out-of-plane orientation of the film. (b) Intensity profile taken along the dashed line in (a) showing that the vdW gaps occur every 1 nm. (c) Low magnification image of the SL. The presence of vdW gaps (dark bands) parallel to the substrate/film interface confirms the textured nature of the SL.

along the dashed line in Fig. 3(a) is shown in Fig. 3(b). The intensity profile shows a structure that repeats itself approximately every 1 nm, indicating that these intensity modulations are due to the 1 nm thick quintuple layers in Sb_2Te_3. Figure 3(c) shows a low magnification image of the superlattice. From this image one can clearly see that the as-grown superlattice also has a well defined interface with the carbon bottom layer and that the surface of the layer is relatively flat. This is consistent with the SEM investigations shown below. Furthermore, horizontal lines can be observed in the image, consistent with the $(0\ 0\ 1)_t$ orientation of the superlattice.

GeTe/Sb_2Te_3 superlattices on SiO_2

After the growth on amorphous carbon the growth on SiO_2 was studied, because of its technological relevance. Figure 4(a) shows a scanning electron microscopy image of the surface of a sample grown on device structures with a SiO_2 surface. It can be seen that the surface is rather rough, which is consistent with the growth of a polycrystalline film. This can also be deduced from the RHEED pattern, shown in Figure 4(b). The RHEED pattern shows rings, indicative of a polycrystalline film. On the other hand SEM images of samples grown on surfaces that were ex situ exposed to Ar+ irradiation were very flat, i.e. Fig. 4(c). The RHEED pattern taken after the deposition, Fig. 4(d), showed streaks indicating that the superlattice has a well-defined out-of-plane orientation, consistent with the observation of Saito et al.[20] A similar improvement of the texture was observed for the irradiation of the substrate surface by electrons from the in situ RHEED electron beam that have an energy of 20 keV, i.e. Fig.4(e)&(f). This demonstrates that Ar^+-ion and electron irradiation alter the surface, so that it is more suited to the growth of 2D materials. This shows that besides the use of an appropriate deposition procedure, the quality of the out-of-plane also depended on the surface preparation.

XPS measurements were performed in order to study the influence of Ar^+ ion irradiation on the SiO_2 surface. In figure 5 the XPS spectra of the Si 2p and 2s core levels of a pristine SiO_2 sample and a SiO_2 sample exposed to Ar^+ irradiation are compared with each other. For pristine SiO_2 a binding energy of 103.8 eV and 154.8 eV are observed for the Si 2p and 2s core levels, respectively, in good agreement with literature values.[23–25] It can be seen that the core levels of the sputter "cleaned" sample are shifted to lower binding energy with respect to the reference sample. Such a shift is typical

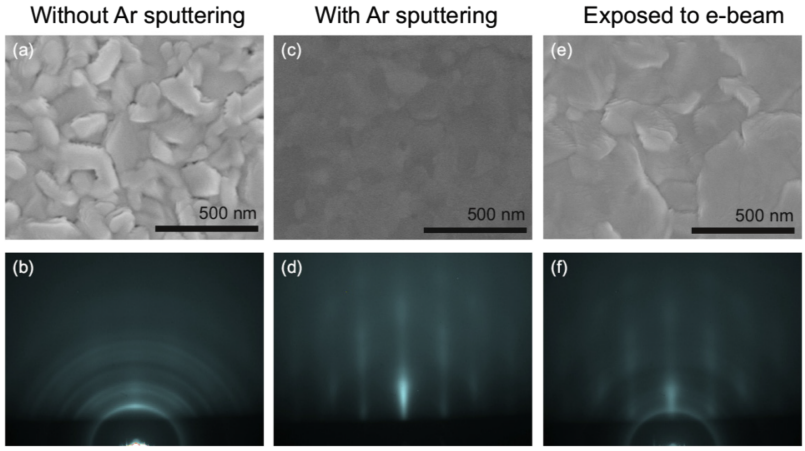

FIG. 4. Effect of surface preparation on the texture of the SL. Comparison of the surface morphology as detected by SEM and RHEED pattern for films grown on a SiO_2 substrate unexposed to Ar^+ ion (a)&(b), a substrate that is exposed to Ar^+ ions (c)&(d) a substrate that is unexposed to Ar^+ ions, but exposed to an 20 keV electron beam (e)&(f).

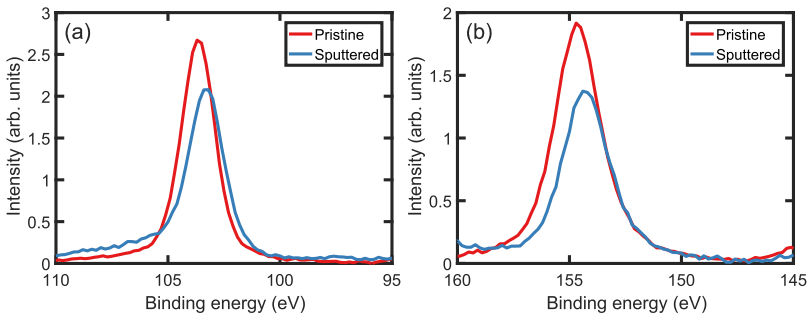

FIG. 5. XPS spectra after background removal around the (a) Si 2p and (b) Si 2s peaks of pristine SiO_2 and SiO_2 that is exposed Ar^+ ions. The shift of the Si 2s and the Si 2p peaks to lower binding energy is attributed to the formation of silicon suboxide during to the sputtering process.

for the reduction of the oxygen content in SiO_2.[24] This indicates that the Ar^+ irradiation resulted in the preferential sputtering of oxygen atoms and hence in the formation of a silicon suboxide (SiO_x) at the SiO_2 surface. We note that the investigated samples were exposed to air for some days, indicating that the SiO_x is stable. High energy electrons, such as the 20 keV electron of the RHEED setup, are also able to sputter light elements.[26] This suggests that SiO_x is also formed due to the exposure to the electron beam of the RHEED setup.

The XPS results thus indicate that the improved texture of Sb_2Te_3 films on sputtered SiO_2 surfaces is due to the formation of SiO_x on the surface. In this respect, it is interesting to note that argon and oxygen sputtering treatments can reduce the contact angle of water on glass and quartz.[27] In general, it can be assumed that the orientation of the Sb_2Te_3 layer is determined by the bonding of Sb_2Te_3 with the underlying layer. For example, the presence of dangling bonds on the Si(111)-(7x7) determines the in-plane orientation of Sb_2Te_3 films.[12] Given the differences in chemistry between SiO_2 and SiO_x one can expect a different bonding with Sb_2Te_3. However, it remains unclear why the bonding with SiO_x results in an improved out-of-plane alignment compared to a bonding with SiO_2. More detailed studies are clearly needed in order to determine the exact origin of the improved texture of Sb_2Te_3 and SL on sputtered SiO_2 surfaces.

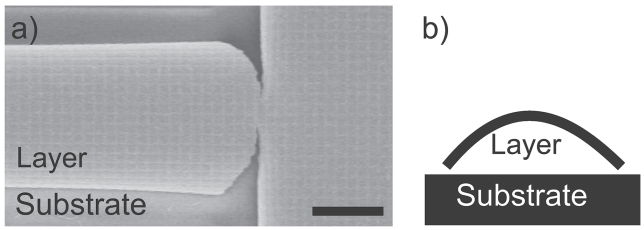

FIG. 6. SEM image showing the delamination of the SL after the deposition of a W capping layer (a). It is observed that the layers are curved inwardly. The scalebar is 10 μm. Schematic cross section of the delaminated layer as seen from the left of the SEM image (b).

Delamination

Finally, it was observed that the deposition of a W capping could result in the delamination of a part of the deposited layers from the substrate, i.e. Fig. 6. Such a delamination was not observed for polycrystalline GST[21] or superlattices with a bad out-of-plane alignment, such as in Fig. 3(a). Delamination can occur when a material is under stress. The curvature of the delaminated layers in Fig. 6 indicates that the W layer was under compressive stress with respect to the SL. Stress can be induced by a difference in thermal expansion coefficient between two materials. However, given the fact that the W layer was deposited at room temperature, it is unlikely that a significant amount of stress develops due a difference in thermal expansion coefficient between the superlattice and W. On the other hand it is known that W films grown under low pressure conditions can be compressively stressed.[28,29] The release of a compressive stress would result in an expansion of the W layer with respect to the superlattice and the delamination of the two layers. This is in good agreement with our observations. We therefore attribute the delamination to the presence of compressive stress in the W capping layer. In order to overcome this fabrication issue, the sputtering power for the W films was reduced from 100 Watt to 50 Watt. The reduction of the sputtering power also reduces the kinetic energy of the W atoms, which is known to reduce the amount of compressive stress in the film.[28,29] With this approach the W growth rate is reduced by approximately 50% and the delamination of the superlattice was prevented. The fact that we did not observe any delamination of polycrystalline films directly relates the delamination with the $(0\,0\,1)_t$ out-of-plane orientation of the superlattices. For such an orientation the bond strength between the superlattice and Argon treated surface or the superlattice and the W layer are likely reduced due to the presence of a vdW gap at the interface. This suggests that delamination due to a reduced bonding strength between 2D bonded materials and other materials will be a common fabrication challenge for the use of 2D bonded materials in electronic devices. This can however be easily overcome by controlling the stress state of subsequent layers grown on top of 2D materials.

CONCLUSIONS

We demonstrated the growth of textured Sb_2Te_3 and $GeTe/Sb_2Te_3$ SL by MBE on conductive as well as insulating amorphous substrates, such as carbon and SiO_2. This was made possible by using an Sb_2Te_3 buffer layer of 5 nm grown at low temperatures. This shows that such textured layers can also be obtained in ultra high vacuum environments and by other means then sputter deposition. In particular we showed that the successful growth on SiO_2 strongly depends on the surface preparation and that the SiO_2 surface is more suitable to the growth of 2D materials after Ar^+ sputtering or exposure to a 20 keV electron beam. We showed that the exposure of SiO_2 to Ar+ results in the formation of silicon suboxide. Furthermore, we observed that delamination can occur when an additional layer is grown on textured 2D materials. We attribute this to the small interaction between 2D materials and other materials due to the presence of vdW bonding and to the presence of compressive stress in the capping layer. We showed that delamination can be overcome by using optimized deposition conditions for the additional layers. We expect that these

results can also be applied to the growth of other 2D materials and will contribute to the integration of 2D materials with CMOS technology and to the realization of future devices based on 2D materials.

ACKNOWLEDGMENTS

This work was supported by European Commission within the FP7 project PASTRY (GA 317746). We thank R.N. Wang, S. Behnke, C. Stemmler, S. Rauwerdink and A.-K. Bluhm for technical support and T. Auzelle for critical reading of the manuscript.

[1] K. S. Novoselov, A. K. Geim, S. V. Morozov, D. Jiang, Y. Zhang, S. V. Dubonos, I. V. Grigorieva, and A. A. Firsov, Science **306**, 666 (2004).
[2] S. Z. Butler, S. M. Hollen, L. Cao, Y. Cui, J. A. Gupta, H. R. Gutiérrez, T. F. Heinz, S. S. Hong, J. Huang, A. F. Ismach, E. Johnston-Halperin, M. Kuno, V. V. Plashnitsa, R. D. Robinson, R. S. Ruoff, S. Salahuddin, J. Shan, L. Shi, M. G. Spencer, M. Terrones, W. Windl, and J. E. Goldberger, ACS Nano **7**, 2898 (2013).
[3] D. Hsieh, Y. Xia, D. Qian, L. Wray, F. Meier, J. Dil, J. Osterwalder, L. Patthey, A. Fedorov, H. Lin, A. Bansil, D. Grauer, Y. Hor, R. Cava, and M. Hasan, Phys. Rev. Lett. **103**, 146401 (2009).
[4] K. S. Novoselov, A. K. Geim, S. V. Morozov, D. Jiang, M. I. Katsnelson, I. V. Grigorieva, S. V. Dubonos, and A. A. Firsov, Nature **438**, 197 (2005).
[5] A. K. Geim and I. V. Grigorieva, Nature **499**, 419 (2013).
[6] J. Momand, R. Wang, J. E. Boschker, M. A. Verheijen, R. Calarco, and B. J. Kooi, Nanoscale **7**, 19136 (2015).
[7] R. Wang, V. Bragaglia, J. E. Boschker, and R. Calarco, Cryst. Growth Des. **16**, 3596 (2016).
[8] B. Casarin, A. Caretta, J. Momand, B. J. Kooi, M. A. Verheijen, V. Bragaglia, R. Calarco, M. Chukalina, X. Yu, J. Robertson, F. Lange, M. Wuttig, A. Redaelli, E. Varesi, F. Parmigiani, and M. Malvestuto, Sci. Rep. **6**, 22353 (2016).
[9] R. E. Simpson, P. Fons, A. V. Kolobov, T. Fukaya, M. Krbal, T. Yagi, and J. Tominaga, Nat. Nanotechnol. **6**, 501 (2011).
[10] R. Venkatasubramanian, E. Siivola, T. Colpitts, and B. O'Quinn, Nature **413**, 597 (2001).
[11] A. Koma, Thin Solid Films **216**, 72 (1992).
[12] J. E. Boschker, J. Momand, V. Bragaglia, R. Wang, K. Perumal, A. Giussani, B. J. Kooi, H. Riechert, and R. Calarco, Nano Lett. **14**, 3534 (2014).
[13] J. C. Koepke, J. D. Wood, C. M. Horvath, J. W. Lyding, and S. Barraza-Lopez, Appl. Phys. Lett. **107**, 71603 (2015).
[14] J. E. Boschker, L. A. Galves, T. Flissikowski, J. M. J. Lopes, H. Riechert, and R. Calarco, Sci. Rep. **5**, 18079 (2015).
[15] N. V. Tarakina, S. Schreyeck, M. Luysberg, S. Grauer, C. Schumacher, G. Karczewski, K. Brunner, C. Gould, H. Buhmann, R. E. Dunin-Borkowski, and L. W. Molenkamp, Adv. Mater. Interfaces **1**, 1400134 (2014).
[16] J. Kampmeier, S. Borisova, L. Plucinski, M. Luysberg, G. Mussler, and D. Grützmacher, Cryst. Growth Des. **15**, 390 (2015).
[17] N. Bansal, N. Koirala, M. Brahlek, M. Han, Y. Zhu, Y. Cao, J. Waugh, D. S. Dessau, and S. Oh, Appl. Phys. Lett. **104**, 241606 (2014).
[18] L. J. Collins-McIntyre, W. Wang, B. Zhou, S. C. Speller, Y. L. Chen, and T. Hesjedal, Phys. Status Solidi **252**, 1334 (2015).
[19] S.-K. Jerng, K. Joo, Y. Kim, S.-M. Yoon, J. H. Lee, M. Kim, J. S. Kim, E. Yoon, S.-H. Chun, and Y. S. Kim, Nanoscale **5**, 10618 (2013).
[20] Y. Saito, P. Fons, A. V. Kolobov, and J. Tominaga, Phys. Status Solidi **252**, 2151 (2015).
[21] J. E. Boschker, M. Boniardi, A. Redaelli, H. Riechert, and R. Calarco, Appl. Phys. Lett. **106**, 23117 (2015).
[22] R. Wang, J. E. Boschker, E. Bruyer, D. Di Sante, S. Picozzi, K. Perumal, A. Giussani, H. Riechert, and R. Calarco, J. Phys. Chem. C **118**, 29724 (2014).
[23] R. Alfonsetti, L. Lozzi, M. Passacantando, P. Picozzi, and S. Santucci, Appl. Surf. Sci. **70–71**, 222 (1993).
[24] F. G. Bell and L. Ley, Phys. Rev. B **37**, 8383 (1988).
[25] T. Gross, M. Ramm, H. Sonntag, W. Unger, H. M. Weijers, and E. H. Adem, Surf. Interface Anal **18**, 59 (1992).
[26] R. Behrisch, *Sputtering by Particle Bombardment II* (Springer, Berlin, Heidelberg, 1983).
[27] L. Eske and D. Galipeau, Colloids Surfaces A Physicochem. Eng. Asp. **154**, 33 (1999).
[28] D. W. Hoffman and J. A. Thornton, Thin Solid Films **45**, 387 (1977).
[29] E. Chason and P. R. Guduru, J. Appl. Phys. **119**, 191101 (2016).